J. Appl. Cryst. (1999). **32**, 1127–1133

Imaging of the helical arrangement of cellulose fibrils in wood by synchrotron X-ray microdiffraction

H. Lichtenegger,[a]* M. Müller,[b] O. Paris,[a] Ch. Riekel[b] and P. Fratzl[a]

[a]*Erich Schmid Institute of Materials Science, Austrian Academy of Sciences and Metal Physics Institute, University of Leoben, Jahnstr. 12, A-8700 Leoben, Austria, and* [b]*European Synchrotron Radiation Facility (ESRF), BP 220, F-38043 Grenoble CEDEX, France. E-mail: fratzl@unileoben.ac.at*

(*Received 16 May 1999; accepted 24 August 1999*)

Abstract

A complete image of the helical arrangement of cellulose fibrils in the S2 layer of adjacent wood cells of *Picea abies* (Norwegian spruce) was obtained by applying position-resolved synchrotron X-ray microdiffraction on cells in cross section. In contrast to conventional fiber diffraction studies, the incident beam was parallel to the longitudinal cell axis, resulting in a glancing angle μ far from 90° with respect to the cellulose fibrils. This special choice of diffraction geometry allowed us to take advantage of an asymmetry effect in the two-dimensional diffraction patterns arising from the curvature of the Ewald sphere to obtain information on the local orientation of the cellulose fibrils. The small size of the beam, smaller than the thickness of a single cell wall, allowed mesh scans over intact transverse sections of adjacent wood cells with a microscopic position resolution. The scan yielded a map of diffraction patterns that could readily serve as a microscopic image. Each of the diffraction patterns was then used to evaluate the local orientation of the cellulose fibrils at the actual beam position. The combination of these results gave an image of cellulose fibrils forming (*Z*) helices in several adjacent wood cells.

1. Introduction

X-ray scattering methods (diffraction and small-angle scattering) are well known to be powerful tools for the determination of the nanostructure of biological materials such as bone or wood. However, one of the main challenges when investigating biological materials with scattering techniques is their hierarchical structure and the resulting inhomogeneity. The investigation of local variations of the nanostructure requires position-resolved scattering techniques (Fratzl *et al.*, 1997; Riekel *et al.*, 1997), the position resolution being limited by the size of the incident X-ray beam. Using conventional X-ray sources, the beam diameter is of the order of typically 0.1 to 1 mm. In the case of a material with a pronounced structure on the micrometre scale, this yields only averaged nanostructural parameters.

The X-ray microbeam obtained from a synchrotron radiation source with a recently developed focusing technique (Riekel *et al.*, 1997) now allows extensive non-destructive scans with a position resolution of 2 μm. Using this technique, one may address new questions concerning the local nanostructure in hierarchical biomaterials such as wood.

On the microscopic scale, wood is a cellular material, consisting of tube-shaped cells with diameters of 20–40 μm and lengths of the order of millimetres. The cell wall is organized in several layers, the largest one (S2) comprising 79–85% of the cell-wall volume (Fengel & Wegener, 1984). On the nanometre scale, the wood cell wall is a fiber composite consisting of an amorphous matrix and partially crystalline cellulose fibrils. In the S2 layer the cellulose fibrils are tilted with respect to the longitudinal cell axis by a sharply defined angle and trace a steep helix around the cell. The tilt angle (microfibril angle) may vary considerably within one individual tree (see for example Preston, 1934; Sahlberg *et al.*, 1997). Using microscopic techniques, the helical orientation of the cellulose fibrils in the S2 layer has been found to be mostly right handed (*Z* helix) (see for example Meylan & Butterfield, 1978) but also a left-handed (*S*) helix has been reported (Jane, 1970; Panshin & De Zeeuw, 1970).

Whereas X-ray scattering methods have been used successfully to determine average structural parameters such as the mean microfibril angle (see for example Cave, 1997; Evans, 1994; Jakob *et al.*, 1994, 1995) or the mean diameter of the cellulose fibrils (Heyn, 1955; Jakob *et al.*, 1994), they have up to now been inappropriate for the investigation of the helical orientation of the cellulose fibrils. The X-ray beam obtained from a conventional laboratory source always irradiated a number of complete cells. Thus, cell walls of all orientations contributed to the scattering signal and right-handed and left-handed helices could not be distinguished. This difficulty may be overcome by using a beam diameter smaller than the cell-wall thickness.

In this paper we combine the microfocus technique with an unusual diffraction geometry for the position-resolved measurement of the local fibril orientation in

intact transverse wood sections. The determination of the local fibril orientation is based on asymmetry effects in the diffraction patterns caused by the curvature of the Ewald sphere. In this paper we explain the experimental concept and present an application for the first direct visualization of the trace of the cellulose fibrils around one complete cell and in adjacent cells.

2. Diffraction geometry

The position-resolved determination of the orientation of the cellulose fibrils requires the definition of the scattering volume in the specimen with a precision better than the beam diameter (2 μm). It is impossible, however, to keep the scattering volume the same when the sample is rotated. For this reason we have devised a method for determining the crystallographic orientation of the cellulose fibrils that avoids any specimen rotation. Following this method, a cross section of wood is placed perpendicular to the X-ray beam and diffraction patterns recorded in transmission. This geometry allows the successive irradiation of small sample volumes containing cellulose fibrils with approximately the same orientation and, thus, the investigation of adjacent wood cells without the need to prepare separate single cell walls (Fig. 1). The information on the cellulose crystallite orientation is gained using the equatorial cellulose reflections. An asymmetry effect in the diffraction patterns may be used for the determination of the fibril orientation, applying the following considerations.

The cellulose crystallites building up the cellulose fibrils in the wood cell wall are monoclinic with their *c* axis [indexing according to Gardner & Blackwell (1974)] parallel to the fibril axis. The strongest reflection is the 020 reflection, occurring in the equatorial plane (*i.e.* perpendicular to the longitudinal fibril axis) at $q = 1.6$ Å^{-1} in reciprocal space; **q** is the scattering vector and $q = |\mathbf{q}| = (4\pi/\lambda)\sin\theta$, where λ is the wavelength of the incoming beam and 2θ is the scattering angle. In the equatorial plane also additional relatively strong and, therefore, easy to observe reflections are found: 110 at $q = 1.17$ Å^{-1} and $1\bar{1}0$ at $q = 1.04$ Å^{-1}. Their positions in reciprocal space are sketched in Fig. 2. The cellulose crystallites are assumed to be randomly oriented about their crystallographic *c* axis. This assumption is essential for the following consideration and it is checked experimentally within the framework of this paper (see §3). Fig. 2 shows the smearing of the equatorial reflections to reflection rings. Only two rings are drawn, because, due to the small crystallite size, the equatorial reflections are considerably broadened and the 110 and the $1\bar{1}0$ reflection rings overlap.

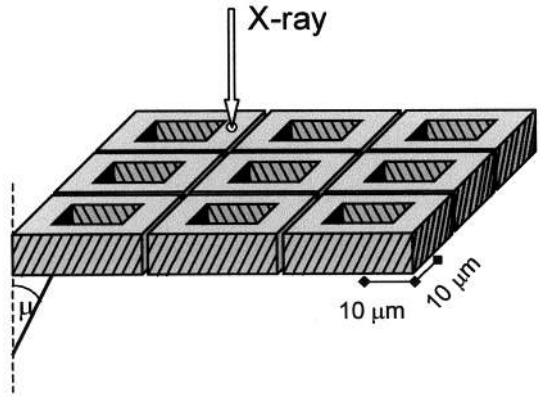

Fig. 1. Wood cells in cross section were scanned by a microbeam smaller than the thickness of a single cell wall. In this geometry, the tilt angle of the cellulose fibrils with respect to the beam simply corresponds to the microfibril angle μ. The sample volume irradiated by the beam is only a part of a single cell wall and, thus, contains mostly parallel cellulose fibrils.

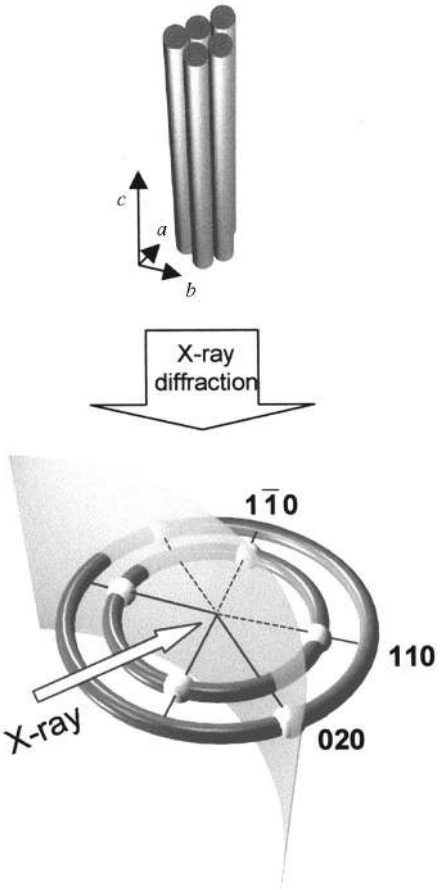

Fig. 2. A perfect alignment of all crystallographic axes of cellulose yields sharp Bragg spots corresponding to the 020, 110 and $1\bar{1}0$ reflections in the plane perpendicular to the fibril axis in reciprocal space. A random orientation of the fibrils around their longitudinal (*c*) axis results in a cylindrical smearing of the reflections to rings. Here only two rings are drawn, because the 110 and the $1\bar{1}0$ reflections overlap as a result of reflection broadening arising from the small crystallite size. In the case of a perfect alignment, the three reflections do not appear simultaneously in a single diffraction pattern, because the Ewald sphere does not intersect all the diffraction spots at the same time.

2.1. *Qualitative description*

In the case of cylindrical smearing of the equatorial reflections around the c axis, the observed diffraction pattern will, according to basic diffraction theory, correspond to an intersection of the Ewald sphere with concentric diffraction rings with radius q and center O, where O is the origin in reciprocal space. This situation is described qualitatively in Fig. 3. The orientation of the cellulose fibril is given by an angle μ with respect to the direction of the incident beam (Fig. 3*a*), and a vector $\mathbf{a}_\varphi$ denoting the orientation in the plane perpendicular to the incident beam, where φ is the angle with respect to a fixed direction perpendicular to the incident beam. The intersection of the equatorial reflection rings in the plane perpendicular to the fibril axis with the Ewald sphere is shown in a three-dimensional sketch in Fig. 3(*b*). The picture already shows qualitatively that the points of intersection A and B, are (i) symmetric about the fibril orientation and (ii), due to the curvature of the Ewald sphere, nearer to each other in the direction opposite the fibril orientation. This becomes more obvious in Fig. 3(*c*), which shows the projection of the intersection points on a plane at right angles to the beam, yielding a diffraction signal at points A' and B'. The pattern is indicative for the orientation of the fibril $\mathbf{a}_\varphi$ in the plane perpendicular to the beam. In the following section, these considerations are quantified.

2.2. *Quantitative description*

In Fig. 4 the diffraction geometry for a scattering pattern as drawn in Fig. 3(*c*) is sketched. First, the points A and B are at a distance q from O, the origin in reciprocal space, where q is the length of the scattering vector of the corresponding Bragg reflection. Moreover, A, B and O are on the Ewald sphere, which implies that the angle between AN and AO must be equal to θ, 2θ being the scattering angle. N is the normal projection of A or B on the beam direction. Since A, B and O are elements of the equatorial reflection plane, the triangle ABO is perpendicular to the cellulose fibril (corresponding to the crystallographic c axis). As a consequence, the angle between OF and ON is $90^\circ - \mu$, where F is the center of AB and μ corresponds to the microfibril angle. Finally, defining η as the angle between NF and NA (or NB, respectively), one obtains the following relations:

$$\overline{NF} = \overline{NA}\,\cos\eta = q\,\cos\theta\,\cos\eta,$$
$$\overline{NF} = \overline{ON}/\tan\mu = q\,\sin\theta/\tan\mu.$$

It follows immediately that

$$\cos\eta = \tan\theta/\tan\mu. \qquad (1)$$

Note that the angle η is defined with respect to NF, which corresponds to the direction $-\mathbf{a}_\varphi = \mathbf{a}_{\varphi+180}$.

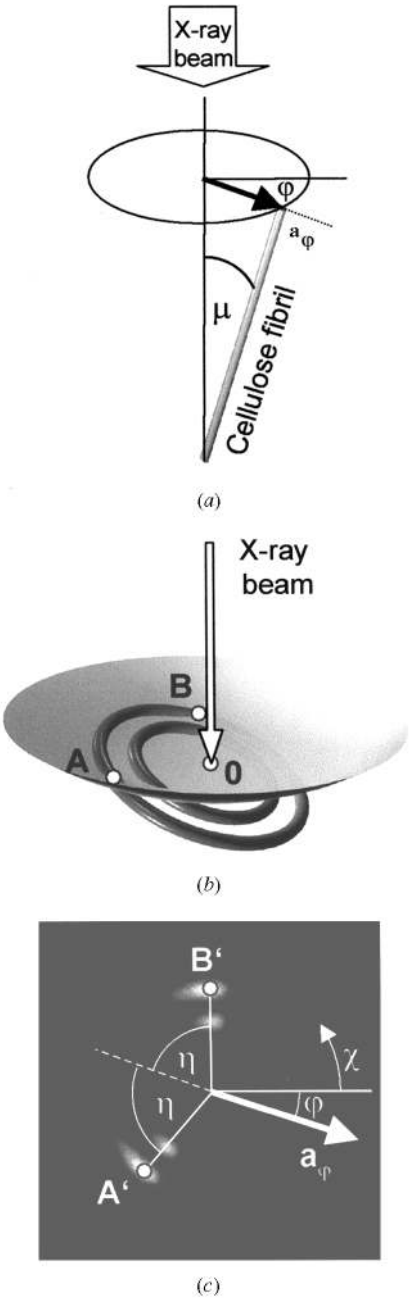

Fig. 3. Basic principle for the measurement of local fibril orientations. (*a*) Cellulose fibril tilted by an angle μ with respect to the incoming X-ray beam; $\mathbf{a}_\varphi$ denotes the orientation of the fibril in the plane perpendicular to the beam. (*b*) In reciprocal space, the Ewald sphere intersects the Debye–Scherrer rings resulting from cylindrical smearing of the Bragg reflections (020: large ring; 110 + $1\bar{1}0$: small ring) around the fibril axis. The smearing is caused by random rotation of parallel cellulose fibrils around their longitudinal axis. The points of intersection are denoted by A and B. O is the origin in reciprocal space. (*c*) Scattering pattern as it would appear on an area detector in the plane perpendicular to the beam. The scattering pattern is asymmetric with signals at A' and B', at $\chi = \varphi + 180^\circ \pm \eta$. The orientation $\mathbf{a}_\varphi$ of the cellulose fibrils (indicated by an arrow) can be extracted directly from the peak positions and coincides with the symmetry axis of the peaks.

Projecting the points of intersection A and B on a two-dimensional detector positioned in a plane perpendicular to the X-ray beam, gives signals at points A' and B' with coordinates (R, χ), where R is the radius in the detector plane given by $R = D \sin(2\theta)$ and D is the sample–detector distance. The azimuth χ in the detector plane where a diffraction signal occurs is given by

$$\chi = \varphi + 180^\circ \pm \eta, \qquad (2)$$

where $\eta = \arccos(\tan\theta/\tan\mu)$ (see also Fig. 3*c*).

For $\theta < \mu$, $\tan\theta/\tan\mu$ would become >1 and there is no solution to equation (2). In other words, the Ewald sphere would not intersect the diffraction ring at all. If, on the contrary, θ was very small, η would approach 90° and the scattering pattern would become symmetric about 180°. This would correspond to scattering in the small-angle regime where the curvature of the Ewald sphere is negligible. In an intermediate range of θ, however, η will be $<90^\circ$, owing to the curvature of the Ewald sphere, and the scattering pattern will be asymmetric (*cf.* Fig. 3*c*). The scattering pattern was simulated numerically using equation (2). In this case, the orientation of the cellulose fibrils $\mathbf{a}_\varphi$ can be easily extracted from the scattering pattern.

3. Experimental

3.1. *Sample preparation*

Small cubes were prepared from *Picea abies* (Norwegian spruce). Radial slices were cut from these cubes and the mean microfibril angles were determined by small-angle X-ray scattering (SAXS) using a laboratory source, as described by Jakob *et al.* (1995) and Reiterer *et al.* (1998).

'Latewood' with a fibril angle of 20° with respect to the longitudinal cell axis was chosen for the determination of the helical orientation. Latewood is built in summer and exhibits a higher density due to cells with a thicker cell wall compared to 'earlywood' grown in spring. The difference in density yields the characteristic annual ring pattern. Here, latewood was chosen because of the thicker cell walls, allowing easier position-resolved measurements of single walls. The cube containing the selected annual ring was embedded in polymethyl methacrylate. Cross sections of 10 μm thickness were cut out of the selected latewood using a microtome. The samples were mounted on copper grids for transmission electron microscopy.

For investigating the orientation of the cellulose crystallites around their c axis, additional samples were cut in the tangential direction out of latewood with fibrils running parallel to the cell axis. Having a thickness of 10 μm, they contained at maximum two adjacent cell walls.

3.2. *X-ray microdiffraction experiments*

X-ray diffraction measurements were carried out at the European Synchrotron Radiation Facility (Grenoble, France), beamline ID 13 (Microfocus). Fig. 5 shows the experimental setup schematically. The X-ray beam (wavelength $\lambda = 0.78$ Å) was focused to a diameter of 2 μm by a glass capillary (Riekel *et al.*, 1997). A guard aperture (Pt–Ir, 10 μm diameter) reduced diffuse scattering from the capillary exit. The total flux at the sample position was of the order of 10^{10} photons s^{-1}. The X-ray source, the sample and the area detector

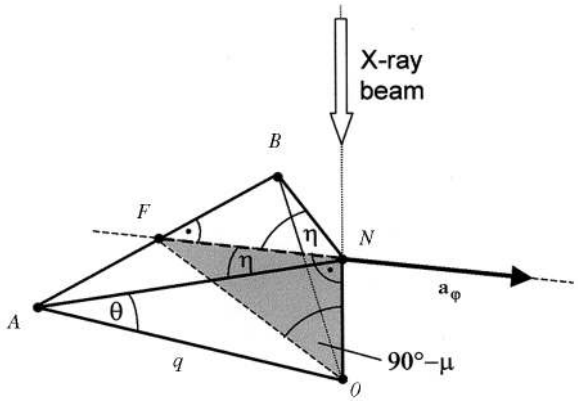

Fig. 4. Diffraction geometry. A and B are the two points of intersection between the equatorial reflection ring and the Ewald sphere. This means that the triangle ABO is tilted by $90^\circ - \mu$ with respect to the incident beam (O is the origin in reciprocal space). According to Bragg's law, $OA = OB = q$ and the angle between OA (respective OB) and NA (respective NB) is θ, where N is the normal projection of A and B onto the direction of the beam and 2θ is the scattering angle. The angle between NA and NB is denoted by 2η. F is the center of AB. $\mathbf{a}_\varphi$ corresponds to the vector defined in Fig. 3(*a*) and denotes the direction of the fibrils in the plane perpendicular to the incident beam.

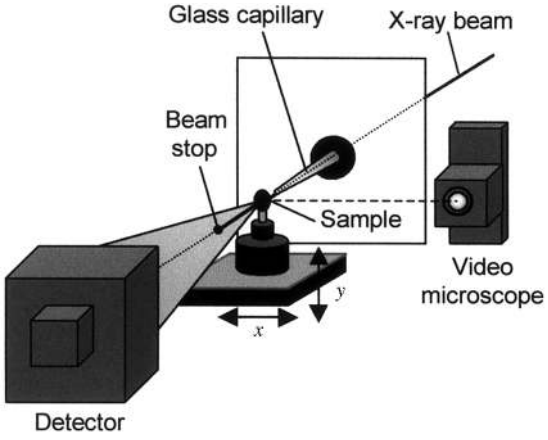

Fig. 5. Experimental setup. The X-ray beam from the synchrotron was focused by an ellipsoidal mirror and a glass capillary to a diameter of 2 μm at the sample position. The sample could be moved in two orthogonal directions perpendicular to the beam by step motors. The scattered signal was recorded by an area detector. A video microscope was used to select the beam position on the sample.

[image-intensified charge-coupled device (CCD) detector] were positioned in one line with a sample–detector distance of 5.2 cm. The sample could be scanned in two orthogonal directions, perpendicular to the beam, with an accuracy of 0.1 μm. The beam position on the sample was selected using an online video microscope. The relation between the position as seen in the microscope and the exact beam position was calibrated using a standard sample. Recording one pattern took only 16 s, so the short time allowed us to carry out extensive mesh scans with a step size of 2 μm in each direction.

In order to check the orientation distribution of the cellulose crystallites around the *c* axis, we performed a rotation experiment using tangential sections with vertically oriented cellulose fibrils. The sample was oriented with the macroscopic cell axis at right angles to the beam (conventional fiber geometry) and rotated around this axis. The intensity ratio of the 020 and 110 + $1\bar{1}0$ reflections was measured. Given the positions of these reflections in reciprocal space (*cf.* Fig. 2), it is obvious that with a beam perpendicular to the fibril axis the Ewald sphere cannot intersect all the reflections simultaneously, unless the reflections are cylindrically smeared around the *c* axis. A constant intensity ratio of the 020 and 110 + $1\bar{1}0$ reflections is indicative of a truly random orientation about the *c* axis.

The cross sections prepared for the determination of the helical fibril orientation were scanned in two orthogonal directions through the beam, and two-dimensional X-ray diffraction patterns were recorded at each point. The beam was parallel to the longitudinal cell axis, and the tilt angle μ of the fibrils with respect to the beam [equation (2)] was simply given by the fibril angle. The beam was considerably smaller in diameter (2 μm) than the thickness of a single cell wall (about 5 μm) and thus hit only a part of a single cell wall at a time (Fig. 1), ensuring that the irradiated sample volume contained mostly parallel cellulose fibrils.

4. Results and discussion

The preparatory rotation experiment using tangential sections in fiber geometry yielded a constant intensity ratio of the 020 and 110 + $1\bar{1}0$ reflections, indicating a random orientation of the cellulose crystallites about their crystallographic *c* axis. This is in accordance with a study by Revol *et al.* (1982) who found a cylindrical smearing of the equatorial cellulose reflections in *Picea mariana* (black spruce) and *Betula verrucosa* (white birch).

The results from the mesh scan over cells in cross section are shown in Figs. 6, 7 and 8. Fig. 6(*a*) is a map of diffraction patterns, combined according to the position where they were collected. As the bright regions showing a scattering signal exactly correspond to cell walls and the dark regions to lumina, the map readily provides a microscopic image of the cross section of one cell in the center and parts of adjacent cells, the pixel size being 2 × 2 μm. In addition, each of the diffraction patterns provides information on the local fibril orientation in the small volume hit by the beam. Fig. 6(*b*)

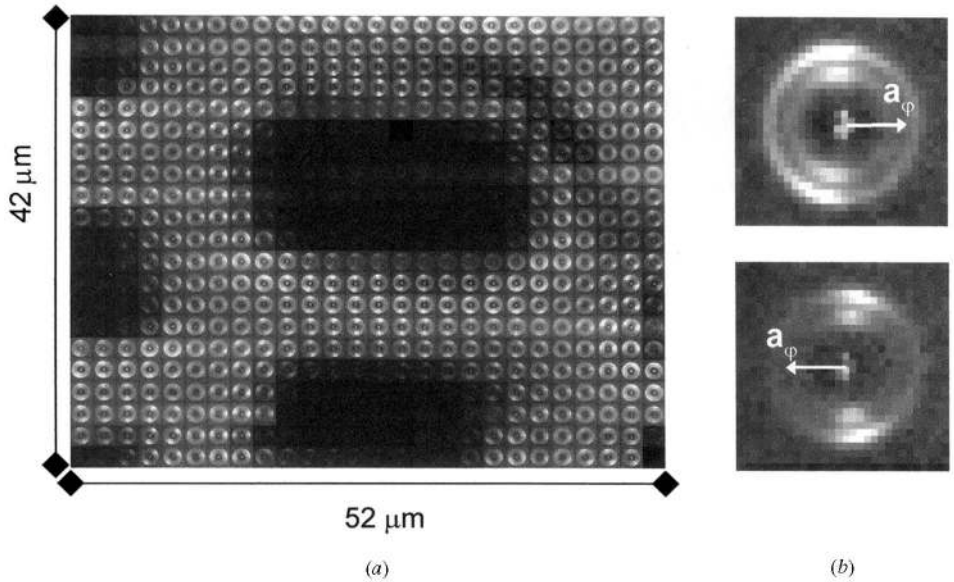

Fig. 6. (*a*) Mesh scan over a complete wood cell in cross section with parts of neighboring cells, pixel size: 2 × 2 μm. Dark regions correspond to lumina, bright regions showing a scattering signal correspond to cell walls. (*b*) Two typical diffraction patterns at greater magnification. Note the asymmetric angular intensity distribution. The direction of asymmetry indicates the local orientation of the cellulose fibrils $\mathbf{a}_\varphi$ (defined in Fig. 3*a*), here denoted by arrows.

shows two typical diffraction patterns at greater magnification. Note that in both the angular intensity distribution is asymmetric, but in different directions.

The orientation of the asymmetric diffraction patterns was used to evaluate the local fibril orientation. The intensity $I(R, \chi)$ was integrated over the radius R in a small region containing the 020 reflection spots (Fig. 7*a*) and plotted *versus* the azimuth χ. The resulting curve showed two pronounced peaks, the positions of which were separated by 2η (Fig. 7*b*). The symmetry axis between the two peaks simply denotes $\varphi + 180^\circ$, where the angle φ indicates the orientation $\mathbf{a}_\varphi$ of the fibril in the plane perpendicular to the incident beam. The arrows in Fig. 6(*b*) correspond to $\mathbf{a}_\varphi$. The length of the arrows is proportional to $90^\circ - \eta$ and thus indicates the extent of asymmetry, which is, for a given reflection and at fixed wavelength, only dependent on the local microfibril angle μ [see equation (2)]. The mean angle determined from the diffraction patterns in this scan was in good agreement with a microfibril angle of 20° as determined by SAXS.

Applying the above procedure to each of the single diffraction patterns, one obtains a map of local orientations which, in combination, represent a complete image of the trace of the cellulose fibrils around the cell (Fig. 8*a*). Translation of the map into a three-dimensional model yields adjacent cells, the S2 layers of which consist of fibrils that are all wound in the same direction and trace a Z helix (Fig. 8*b*). The same helical orientation was found in two other measurement series, each of them covering approximately the same number of cells as in the mesh scan presented here. One series was carried out on a different sample prepared from a different annual ring, but taken from the same tree. Invariably, all cells exhibited the same winding direction.

5. Conclusions

Our results demonstrate that the combination of a novel technique (synchrotron X-ray microdiffraction) with an unusual diffraction geometry makes it possible to visualize (for the first time) the complete trace of cellulose spirals in an intact transverse section of adjacent wood cells. The new experimental concept is based on the combination of several important factors, as follows.

(*a*) The position resolution must be small enough to resolve the structure at the micrometre level; here, the single cell walls. This was achieved by the use of a microbeam from the synchrotron, of which the photon flux density, in spite of the tiny beam diameter, was high enough to obtain good counting statistics in a short time.

(*b*) The scanning facility must allow mesh scans with a pixel size comparable to the beam size; here, 2×2 μm. This technique is most interesting because the map of diffraction patterns may serve already as a microscope image. It provides information on two length scales simultaneously: on the micrometre scale through the microscopic position resolution of the scan and on the nanometre scale through the diffraction patterns recorded at each point. As a consequence, there is no need to take an extra light microscopic image and correlate the diffraction pattern with the position. The correlation with an additional image is always uncertain and, thus, not really suitable for the investigation of hierarchical structures like wood.

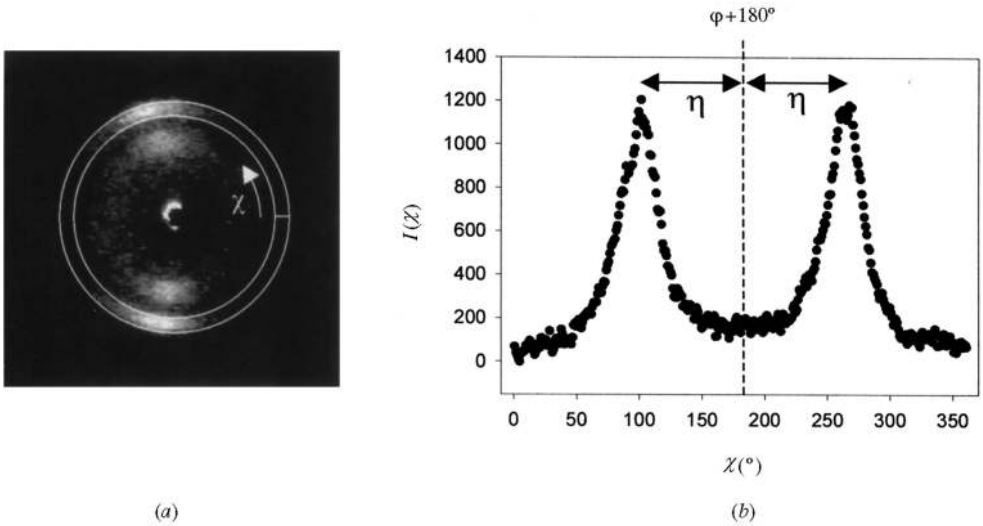

Fig. 7. Evaluation of diffraction patterns. The intensity in the two-dimensional diffraction pattern (*a*) was integrated in the region between the two circles containing the 020 reflection and plotted *versus* χ (*b*). The curve $I(\chi)$ shows two sharp peaks, the maxima of which are separated by 2η. The symmetry axis between the peaks denotes $\varphi + 180^\circ$.

(*c*) The wavelength must be chosen appropriately with regard to the fibril angle in the wood sample to ensure clearly asymmetric scattering patterns. Note that an asymmetry arising from the curvature of the Ewald sphere may occur in every scattering experiment using an area detector, except at very small scattering angles. Here, just this effect is used for the determination of the local fibril orientation in the irradiated sample volume.

This combination provides a powerful imaging tool that will be useful to address other questions concerning the nanostructure of the wood, like the local distribution of microfibril angles within the different layers of a single wood cell wall. Furthermore, it will probably, with some adaptations, open up new possibilities for the investigation of other complex biological or biomimetic fiber composites.

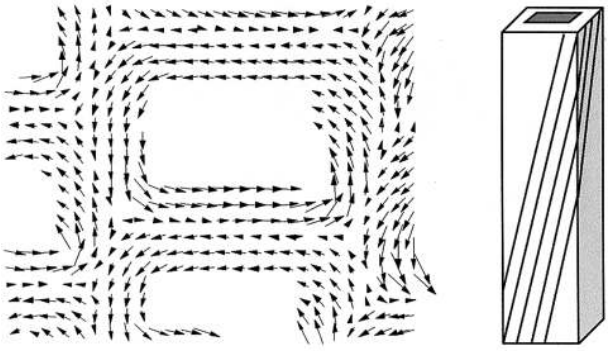

Fig. 8. (*a*) Map of local cellulose fibril orientations. Following the arrows readily yields the trace of the fibrils around the cell. Longer arrows denote a more pronounced asymmetry of the diffraction patterns corresponding to smaller local fibril angles; shorter arrows denote larger fibril angles. (*b*) Translation of the arrow map into a three-dimensional model: the cellulose fibrils trace a *Z* helix around the cell.

We are grateful to G. Dinst, Ludwig-Boltzmann-Institute of Osteology, Wien, for the specimen preparation. We thank the Fonds zur Förderung der Wissenschaftlichen Forschung (FWF Project 10729-BIO) for financial support.

References

Cave, I. D. (1997). *Wood Sci. Technol.* **31**, 143–152, 225–234.
Evans, R. (1994). *Holzforschung*, **48**, 168–172.
Fengel, D. & Wegener, G. (1984). *Wood Chemistry, Ultrastructure, Reaction.* Berlin: De Gruyter.
Fratzl, P., Jakob, H. F., Rinnerthaler, S., Roschger, P. & Klaushofer, K. (1997). *J. Appl. Cryst.* **30**, 765–769.
Gardner, K. H. & Blackwell, J. (1974). *J. Biopolym.* **13**, 1975–2001.
Heyn, A. N. (1955). *J. Appl. Phys.* **26**, 519–526.
Jakob, H. F., Fengel, D., Tschegg, S. E. & Fratzl, P. (1995). *Macromolecules*, **26**, 8782–8787.
Jakob, H. F., Tschegg, S. E. & Fratzl, P. (1994). *J. Struct. Biol.* **113**, 13–22.
Jane, F. W. (1970). *The Structure of Wood*, p. 478. London: A. and C. Black.
Meylan, B. A. & Butterfield, B. G. (1978). *Wood Sci. Technol.* **12**, 219–222.
Panshin, A. J. & De Zeeuw, C. (1970). *Textbook of Wood Technology*, Vol. 1, p. 705. NewYork: McGraw-Hill.
Preston, R. D. (1934). *Philos. Trans. B*, **224**, 131–172.
Reiterer, A., Jakob, H. F., Stanzl-Tschegg, S. E. & Fratzl, P. (1998). *Wood Sci. Technol.* **43**, 335–345.
Revol, J. F., Gancet, Ch. & Goring, D. (1982). *Wood Sci.* **14**, 120–126.
Riekel, C., Cedola, A., Heidelbach, F. & Wagner, K. (1997). *Macromolecules*, **30**, 1033–1037.
Sahlberg, U., Salmon, L. & Oscarsson, A. (1997). *Wood Sci. Technol.* **31**, 77–86.